Journal of Alloys and Compounds 509 (2011) 4053–4059

Contents lists available at ScienceDirect

Journal of Alloys and Compounds

journal homepage: www.elsevier.com/locate/jallcom

Synthesis and characterization of MWCNTs/$Co_{1-x}Zn_xFe_2O_4$ magnetic nanocomposites and their use in hydrogels

Ying Chen [a], Xinwei Wang [a], Qinghong Zhang [b], Yaogang Li [a,*], Hongzhi Wang [b,*]

[a] State Key Laboratory for Modification of Chemical Fibers and Polymer Materials, Donghua University, People's Republic of China
[b] College of Materials Science and Engineering, Donghua University, Shanghai 201620, People's Republic of China

ARTICLE INFO

Article history:
Received 7 September 2010
Received in revised form 1 January 2011
Accepted 3 January 2011
Available online 5 January 2011

Keywords:
Solvothermal method
MWCNT
Co–Zn ferrite
Nanocomposite
Magnetic measurement

ABSTRACT

A novel magnetic nanocomposite of multiwalled carbon nanotubes (MWCNTs) decorated with $Co_{1-x}Zn_xFe_2O_4$ nanocrystals was synthesized successfully by an effective solvothermal method. The as-prepared MWCNTs/$Co_{1-x}Zn_xFe_2O_4$ magnetic nanocomposite was used for the functionalization of P/H hydrogels as a prototype of device to show the potential application of the nanocomposites. The nanocomposites were characterized by X-ray diffraction analysis, transmission electron microscopy and vibrating sample magnetometer. The results show that the saturation magnetization of the MWCNTs/$Co_{1-x}Zn_xFe_2O_4$ magnetic nanocomposites increases with x when the Zn^{2+} content is less than 0.5, but decreases rapidly when the Zn^{2+} content is more than 0.5. The saturation magnetization as a function of Zn^{2+} substitution reaches a maximum value of 57.5 emu g^{-1} for $x = 0.5$. The probable synthesis mechanism of these nanocomposites was described based on the experimental results.

1. Introduction

One of the most exciting classes of nanomaterials is represented by the carbon nanotubes (CNTs), which are at the center of the nanotechnology research [1,2]. Because of their extraordinary properties, such as mechanical, electric, thermal and structural properties, CNTs can be considered as an ideal building block in hybrid materials [3–5]. Although still in a very early stage of research, the dispersion of metal oxides onto CNTs, forming hybrid materials, could show exceptional performance in many applications. For example, anode materials of lithium-ion batteries (SnO_2/MWCNTs nanocomposites) [6], electrode and electrolyte materials of supercapacitors and other electrochemical energy storage/conversion devices (MnO_2/CNTs and ZnO/CNTs nanocomposites) [7,8], optical limiting application (MWCNTs/SiO_2 bulk materials) [9], ceramic products with good mechanical and tribological properties (CNT(Ni)–Al_2O_3 and CNT/aluminosilicate composites) [10,11], etc.

Co–Zn ferrites, one kind of functional spinels composed of mixed metallic oxides with a general formula AB_2O_4 [12,13], exhibit important properties such as excellent chemical stability, high corrosion resistivity, magneto crystalline anisotropy, magnetostriction and magneto optical properties [14]. Co–Zn ferrites have aroused increasing interest among researchers of various fields due to their extensive applications such as information storage system, medical diagnostics, magnetic drug delivery, hyperthermia for cancer treatment, ferrofluid technology, hard disc recording media, flexible recording media, magnetic static wave devices, surface acoustic wave transducers, vacuum seals [14–18]. Various preparation techniques have been developed to produce $Co_{1-x}Zn_xFe_2O_4$ nanoparticles, such as co-precipitation method [19,20], ceramic technique [21], solid-state reaction technique [22,23], forced hydrolysis method [16], hydrothermal route [18] and solvothermal method [24].

Recently, in order to possess the properties of the individual components with a synergistic effect, composite materials based on the integration of CNTs and ferrite have gained growing interest. Shi et al. [25] synthesized Fe_3O_4/CNTs nanocomposites using ethylene glycol as a reductant under 160 °C. After annealing treatment at different temperatures, the average particle size of Fe_3O_4 was increased with increasing temperature and their size distribution was wider at a higher temperature. Chen et al. [26] prepared $ZnFe_2O_4$/MWCNTs composite via a hydrothermal process. The presence of MWCNTs improved the photocatalytic activity of $ZnFe_2O_4$ significantly. Jiang et al. [27] prepared $CoFe_2O_4$/CNTs magnetic nanocomposites by solvothermal method and showed that the nanocomposites were superparamagnetic at room temperature and have a saturation magnetization of 29.6 emu g^{-1}. Lamastra et al. [28] produced a kind of $CoFe_2O_4$/MWCNTs nanofiber by electrospinning a dispersion of MWCNTs in a solution of polyvinylpyrrolidone, iron nitrate nonahydrate, cobalt acetate tetrahydrate, absolute ethanol and H_2O. Liu et al. [29] deco-

* Corresponding authors. Tel.: +86 21 67792342; fax: +86 21 67792340.
E-mail addresses: yaogang_li@dhu.edu.cn (Y. Li), wanghz@dhu.edu.cn (H. Wang).

0925-8388/$ – see front matter © 2011 Elsevier B.V. All rights reserved.
doi:10.1016/j.jallcom.2011.01.018

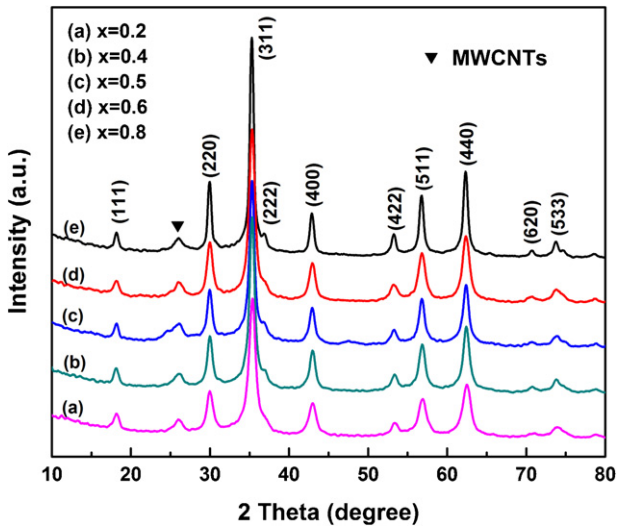

Fig. 1. The XRD patterns of MWCNTs/$Co_{1-x}Zn_xFe_2O_4$ nanocomposites with different compositions (x = 0.2, 0.4, 0.5, 0.6, 0.8).

rated CNTs with nearly monodispersed $M^{II}Fe_2O_4$ (MFe_2O_4, M = Fe, Co, Ni) nanoparticles by *in situ* high-temperature hydrolysis, and the saturation magnetization of Fe_3O_4/CNTs, $CoFe_2O_4$/CNTs and $NiFe_2O_4$/CNTs are obtained as 43.5, 29.6 and 41.7 emu g^{-1}, respectively. Zhang et al. [30] demonstrated a general, efficient and environmentally friendly synthetic strategy for obtaining $Mn_{1-x}Zn_xFe_2O_4$/MWCNTs nanocomposites via a simple solvothermal method. In our previous work, we prepared a series of magnetic monodisperse Co–Zn ferrite nanospheres, which displayed a highest saturation magnetization value of 64.6 emu g^{-1} corresponding to the sample of $Co_{0.5}Zn_{0.5}Fe_2O_4$ nanospheres [24]. Therefore, magnetic Co–Zn ferrite nanospheres are chosen to decorate MWCNTs, in order to improve the magnetic property of the MWCNTs.

Considering the outstanding properties of MWCNTs and $Co_{1-x}Zn_xFe_2O_4$ nanospheres, MWCNTs decorated with $Co_{1-x}Zn_xFe_2O_4$ would have potential applications in many aspects [29,30], for example, the functionalization of hydrogels. Poly(N-isopropylacrylamide) (PNIPAAm) hydrogels are widely utilized in functional hydrogels, which exhibit a clear volume phase transition in response to external stimuli such as temperature, pH, solvent composition, salt concentration, light, mechanical stress and magnetic field [31]. Liu et al. [32] successfully synthesized a series of high hectorite content nanocomposites PNIPAAm/hectorite

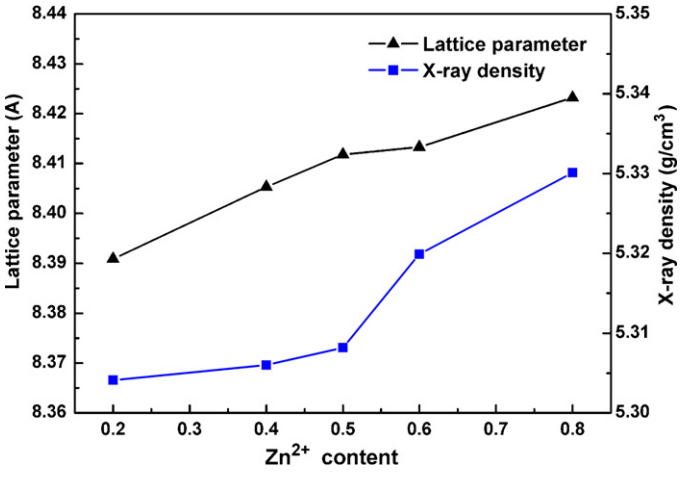

Fig. 2. Lattice parameters and X-ray density of MWCNTs/$Co_{1-x}Zn_xFe_2O_4$ nanocomposites with various Zn^{2+} content.

Table 1
X-ray density and lattice parameters derived from X-ray diffraction pattern of $Co_{1-x}Zn_xFe_2O_4$ nanoparticles with various Zn^{2+} concents.

Zn^{2+} content	0.2	0.4	0.5	0.6	0.8
Lattice parameter a (Å)	8.3909	8.4053	8.4099	8.4133	8.4232
X-ray density (g/cm^3)	5.3041	5.3060	5.3119	5.3199	5.3301

(P/H) hydrogels by choosing a special kind of hectorite (Laponite XLS) modified by tetrasodium pyrophosphate. These hydrogels show surprising mechanical properties and complicated deswelling behavior. Referring to Liu's work [32], the as-prepared MWCNTs/$Co_{1-x}Zn_xFe_2O_4$ magnetic nanocomposites were used for the functionalization of P/H hydrogels as a prototype of device to show the potential application of the nanocomposites.

In this work, we describe a novel, facile, and environmentally friendly synthetic strategy for obtaining MWCNTs/$Co_{1-x}Zn_xFe_2O_4$ magnetic nanocomposites via a solvothermal method. The magnetic properties as well as the microstructures of the nanocomposites have been systematically investigated. Up to now, there are few reports on synthesizing the magnetic nanocomposites of MWCNTs/$Co_{1-x}Zn_xFe_2O_4$, which have a high saturation magnetization. The magnetic properties of the nanocomposites prepared by the solvothermal method were improved greatly compared to other works [27,29]. Furthermore, the MWCNTs/$Co_{1-x}Zn_xFe_2O_4$ magnetic nanocomposite functionalized P/H hydrogels were prepared for the first time and expected to be used as a light-driven and magnetic controlled switch in microreactors.

2. Experimental

2.1. Materials

MWCNTs (length 5 μm; o.d. 50–90 nm; purity: 95–98%) were purchased from Shenzhen Nanotech Port Ltd. Co. (Shenzhen, China). Hectorite-Laponite XLG was purchased from Guangzhou Owen Trade Ltd. Co. (Guangzhou, China). PNIPAAm (purity: 99%) was purchased from J&K Chemical Ltd. The other chemicals, such as hydrated cobalt nitrate ($Co(NO_3)_2{\cdot}6H_2O$), hydrated zinc nitrate ($Zn(NO_3)_2{\cdot}6H_2O$), hydrated iron chloride ($FeCl_3{\cdot}6H_2O$), nitric acid (HNO_3), sodium acetate (NaAc), ethylene glycol (EG), polyethylene glycol (PEG), N,N,N′,N′-tetramethyldiamine (TEMED), and potassium persulfate (KPS), were analytical grade and acquired from Sinopharm Chemical Reagent Co., Ltd.

2.2. Covalent modification of MWCNTs

First, 0.15 g pristine MWCNTs were dispersed into concentrated nitric acid at 100 °C with constant stirring for 24 h. Then, the mixture was diluted with distilled water and rinsed for several times until the pH value reached neutral. Afterwards, the resulting MWCNTs were separated by centrifugation and dried in an oven at 60 °C for subsequent use.

2.3. Synthesis of MWCNTs/$Co_{1-x}Zn_xFe_2O_4$ nanocomposites

MWCNTs/$Co_{1-x}Zn_xFe_2O_4$ magnetic nanocomposites were obtained via a facile solvothermal synthetic route. A series of MWCNTs/$Co_{1-x}Zn_xFe_2O_4$ magnetic nanocomposites were synthesized with different compositions ($0 < x < 1$) under the same conditions. The typical preparation process of MWCNTs/$Co_{1-x}Zn_xFe_2O_4$ (x = 0.2, 0.4, 0.5, 0.6 and 0.8) nanocomposites was described as follows: MWCNTs after acid treated were ultrasonically dispersed in 40 ml ethylene glycol for 30 min. After that, $FeCl_3{\cdot}6H_2O$, $Zn(NO_3)_2{\cdot}6H_2O$ and $Co(NO_3)_2{\cdot}6H_2O$ were dissolved in the resulting MWCNT dispersion according to a certain stoichiometric ratio (5 mmol $FeCl_3{\cdot}6H_2O$, 1.25 mmol $Zn(NO_3)_2{\cdot}6H_2O$ and 1.25 mmol $Co(NO_3)_2{\cdot}6H_2O$ were needed in the case of $Co_{0.5}Zn_{0.5}Fe_2O_4$ and similar for the other value of x). Then, 3.6 g of NaAc and 1 ml of PEG were dissolved in the above mixture solution and vigorously stirred at room temperature for 30 min. Subsequently, the mixture was sealed in a teflon-lined stainless steel autoclave and maintained at 200 °C for 12 h. After reaction, the mixture was cooled to room temperature. The black product was collected by magnet and rinsed with deionized water and ethanol until there were no chloride ions in the solution. Finally, the obtained product was dried in vacuum at 60 °C for 12 h.

2.4. Synthesis of PNIPAAm/MWCNTs/$Co_{1-x}Zn_xFe_2O_4$ hydrogels

PNIPAAm/MWCNTs/$Co_{1-x}Zn_xFe_2O_4$ hydrogels were prepared by simple mixing and solution polymerization. The ratios of raw materials for syntheses of PNIPAAm/MWCNTs/$Co_{1-x}Zn_xFe_2O_4$ hydrogels (P/H/M gels) were as

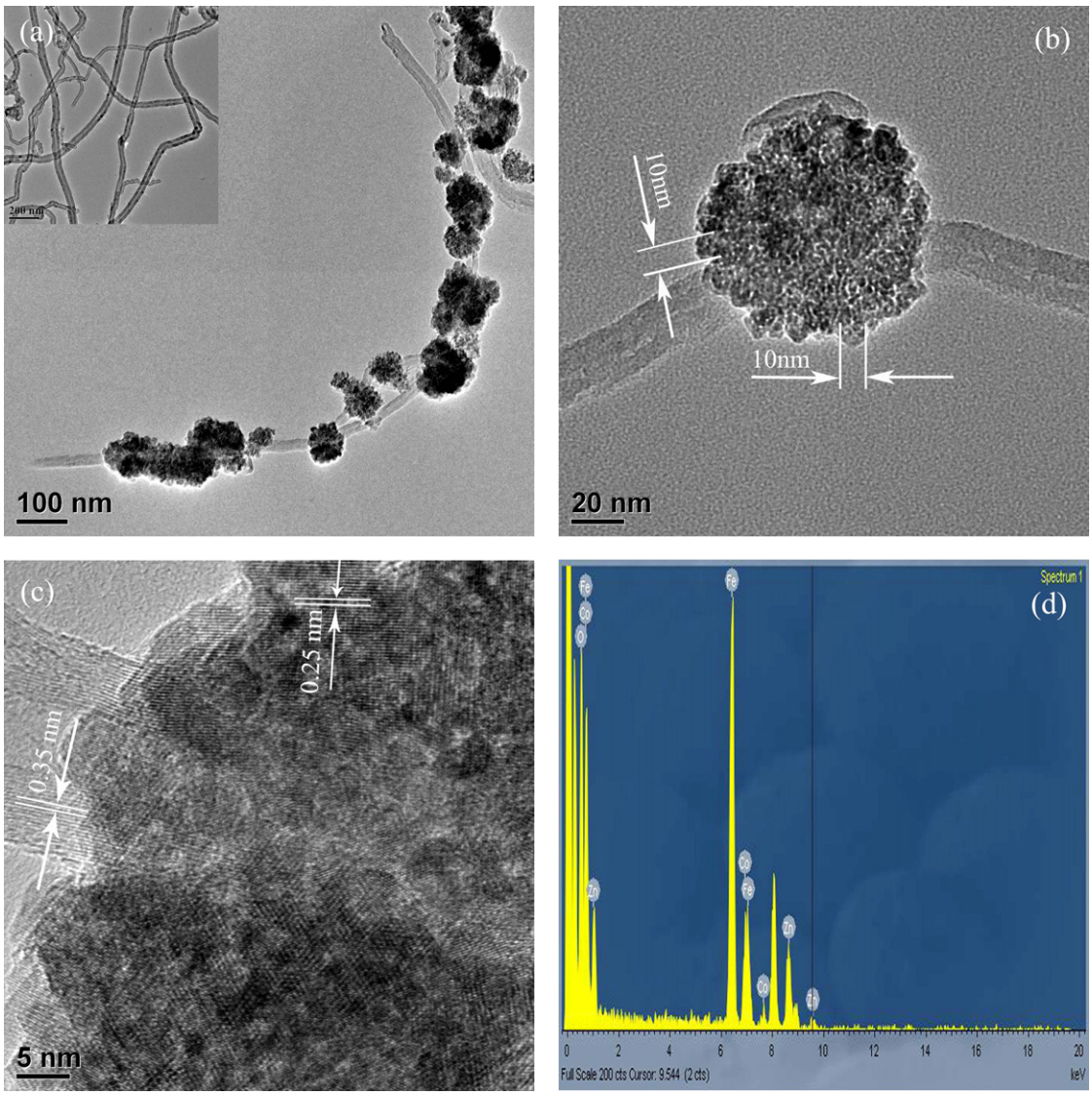

Fig. 3. (a) TEM image of MWCNTs/$Co_{0.5}Zn_{0.5}Fe_2O_4$ nanocomposite and the inset is the pristine MWCNTs; (b) TEM image of MWCNTs/$Co_{0.5}Zn_{0.5}Fe_2O_4$ nanocomposite; (c) HRTEM image of MWCNTs/$Co_{0.5}Zn_{0.5}Fe_2O_4$ nanocomposite; and (d) EDX spectrum of MWCNTs/$Co_{0.5}Zn_{0.5}Fe_2O_4$ nanocomposite.

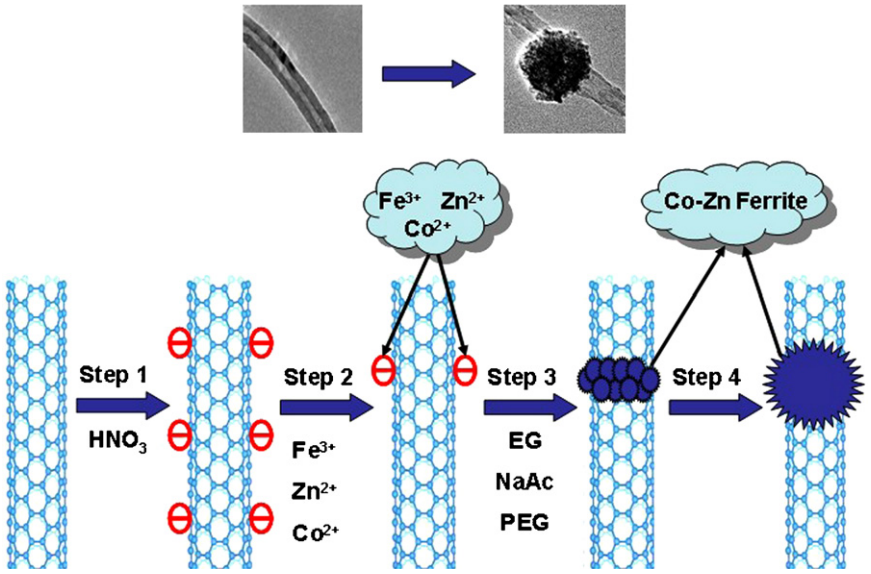

Fig. 4. Schematic diagram of the synthesis of MWCNTs/$Co_{1-x}Zn_xFe_2O_4$ magnetic nanocomposites.

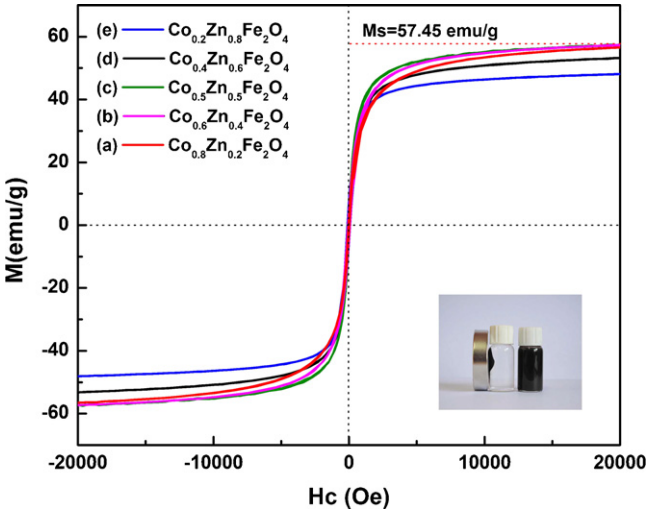

Fig. 5. Magnetic hysteresis loops of MWCNTs/$Co_{1-x}Zn_xFe_2O_4$ magnetic nanocomposites at room temperature. The inset is the sample placed in an external magnetic field.

follows: H_2O/PNIPAAm/hectorite-Laponite XLG/MWCNTs/$Co_{1-x}Zn_xFe_2O_4$/TEMED/KPS = 2 ml: 0.2 g: 0.02 g: 0.02 g: 24 μl: 0.03 g, according to Liu's work [32]. The mixed solution was stirred at 0 °C. After that, free-radical polymerization was carried out at 5 °C for 72 h.

2.5. Characterization

The crystalline phase of the synthesized samples was confirmed by an X-ray powder diffraction (XRD, D/max 2550 V, Rigaku, Japan) with Cu Kα radiation (λ = 1.54056 nm). The size and morphology of the as-synthesized products were observed by transmission electron microscopy (TEM, JEM 2100, JEOL, Japan) with an accelerating voltage of 200 kV. High-resolution transmission electron microscope (HRTEM) images were taken on the same apparatus to determine further details of the nanocomposites. And the $Co^{2+}/Zn^{2+}/Fe^{3+}$ atomic ratio of the MWCNTs/$Co_{1-x}Zn_xFe_2O_4$ was confirmed via energy-dispersive X-ray (EDX) spectrum. Magnetic properties of samples were conducted on a vibrating sample magnetometer (VSM, PPMS Model 6000) in the field of ±4 kOe at room temperature.

3. Results and discussion

3.1. X-ray diffraction analysis

The typical XRD patterns of MWCNTs/$Co_{1-x}Zn_xFe_2O_4$ magnetic nanocomposites are shown in Fig. 1. The diffraction peaks are assigned to MWCNTs at $2\theta = 26°$ [33] in these curves, indicating that the MWCNT structure is not changed in the process of solvothermal treatment. The diffraction peaks of (1 1 1), (2 2 0), (2 2 2), (3 1 1), (4 0 0), (4 2 2), (4 4 0), (5 1 1), (5 3 3) and (6 2 0) crystal planes are indexed to pure $Co_{1-x}Zn_xFe_2O_4$ phase according to the standard JCPDS card No.22-1086 ($CoFe_2O_4$). No impurity peaks were detected, which indicated that high purity crystalline $Co_{1-x}Zn_xFe_2O_4$ was synthesized.

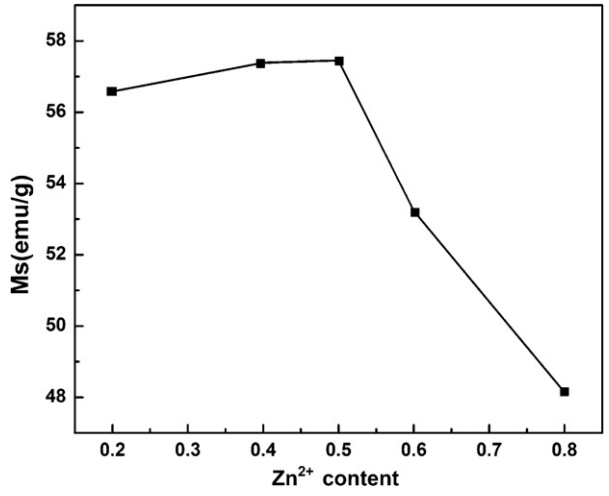

Fig. 6. Saturation magnetizations of MWCNTs/$Co_{1-x}Zn_xFe_2O_4$ magnetic nanocomposites with various Zn^{2+} contents.

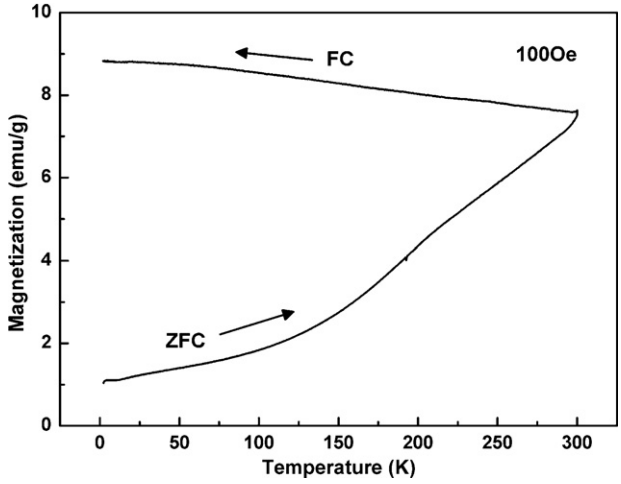

Fig. 7. Temperature dependence of zero field cooled (ZFC) and field cooled (FC) magnetization of MWCNTs/$Co_{0.5}Zn_{0.5}Fe_2O_4$ nanocomposite measured in the presence of 100 Oe applied field.

The XRD data were used to determine lattice constant '*a*' of all the samples of the MWCNTs/$Co_{1-x}Zn_xFe_2O_4$ nanocomposites. The lattice constant was calculated using inter-planar spacing (*d*) values and Miller indices (h k l) values, with an accuracy of ±0.002 Å [22]. The X-ray density (*dx*) was computed from the values of the lattice parameter using the equation $dx = 8M/Na^3$, where *M* is the molecular mass of the sample, *N* is Avogadro's number and '*a*' is the lattice parameter [34]. The values of lattice constant and X-ray density are given in Table 1. Fig. 2 shows that lattice constant and X-ray density increase with increasing Zn^{2+} content. The reason for the increase of lattice parameter values may be due to the larger ionic radii of Zn^{2+} (88 pm) as compared to Co^{3+} (83.8 pm). And the same increase of X-ray density is due to the heavier weight of zinc atom as compared to that of cobalt atom [34].

3.2. Transmission electron microscope analysis

The size and morphology of MWCNTs/$Co_{1-x}Zn_xFe_2O_4$ magnetic nanocomposites were observed by TEM. Here we take the results of MWCNTs/$Co_{0.5}Zn_{0.5}Fe_2O_4$ nanocomposite as the example. Fig. S1a and b shows the morphology of unmodified MWCNTs coated with $Co_{0.5}Zn_{0.5}Fe_2O_4$ magnetic nanospheres. Fig. 3a shows the morphology of covalently modified MWCNTs (inset) and the MWCNTs coated with large quantity of $Co_{0.5}Zn_{0.5}Fe_2O_4$ magnetic nanospheres. Obviously, the structure of MWCNTs remained unchanged in the nanocomposites and magnetic nanospheres of $Co_{0.5}Zn_{0.5}Fe_2O_4$ (about 100 nm in diameter) were successfully synthesized. However, compared to the covalently modified MWCNTs, the unmodified MWCNTs were coated with few $Co_{0.5}Zn_{0.5}Fe_2O_4$ magnetic nanospheres and agglomerated seriously (Fig. S1a). What's more, there are a number of free $Co_{0.5}Zn_{0.5}Fe_2O_4$ magnetic nanospheres around the unmodified MWCNTs (Fig. S1b). In Fig. 3b, it can be clearly seen that the MWCNT passed through the middle of the $Co_{0.5}Zn_{0.5}Fe_2O_4$ magnetic nanosphere. And the grain size of the $Co_{0.5}Zn_{0.5}Fe_2O_4$ nanoparticle is approximately 10 nm. HRTEM micrograph of the sample (Fig. 3c) shows that the fringe spac-

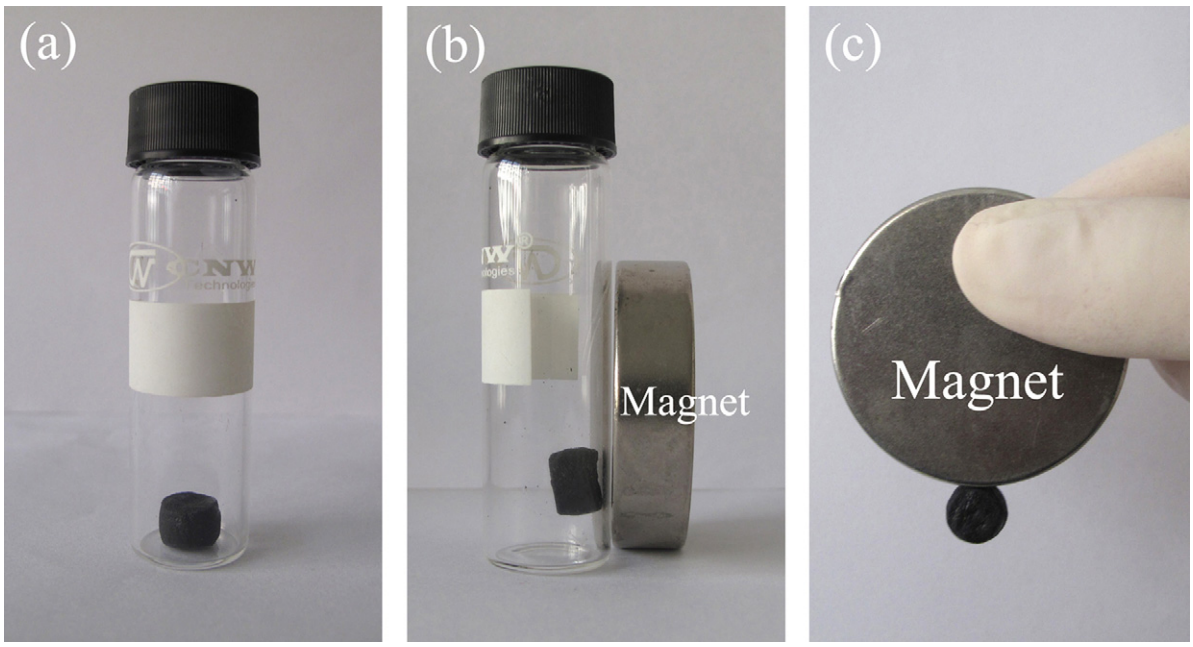

Fig. 8. Photographic image of the response of the PNIPAAm/MWCNTs/$Co_{1-x}Zn_xFe_2O_4$ gel to a magnet.

ing between two carbon layers of MWCNT is about 0.35 nm and (3 1 1) lattice spacing of $Co_{0.5}Zn_{0.5}Fe_2O_4$ nanocrystallite is close to 0.25 nm. Fig. 3d is the EDX spectrum of MWCNTs/$Co_{0.5}Zn_{0.5}Fe_2O_4$ nanocomposite, the result shows that the nanocomposite contains Co, Zn, Fe, O, and C and no contamination element was detected. Moreover, the measured atomic ratio between Fe, Co and Zn (5:1:1) confirms the chemical formula of Co–Zn ferrite is consistent with the experimental stoichiometric.

3.3. Synthesis mechanism

Fig. 4 shows the four-step synthesis process of MWCNTs/$Co_{1-x}Zn_xFe_2O_4$ magnetic nanocomposites. After covalently modified by co- ncentrated nitric acid, the surface of MWCNTs were adhered by carbonyl and carboxyl groups, which was demonstrated to be an efficient method for increasing solubility and chemical reactivity of MWCNTs (step 1) [5]. This process also played an important role on the deposition of metal ions. Co^{2+}, Zn^{2+} and Fe^{3+} were added in the reaction solution, and then adhered on the surface of MWCNTs with high density of carbonyl and carboxyl groups due to electrostatic interaction (step 2). During the solvothermal process, Co–Zn ferrite nanocrystallites were formed along the tube walls of MWCNTs (step 3). And finally, the nanocrystallites grew into spherical aggregation (step 4). In our system, the main driving force for the oriented aggregation of nanocrystals is attributed to the tendency to decrease the high

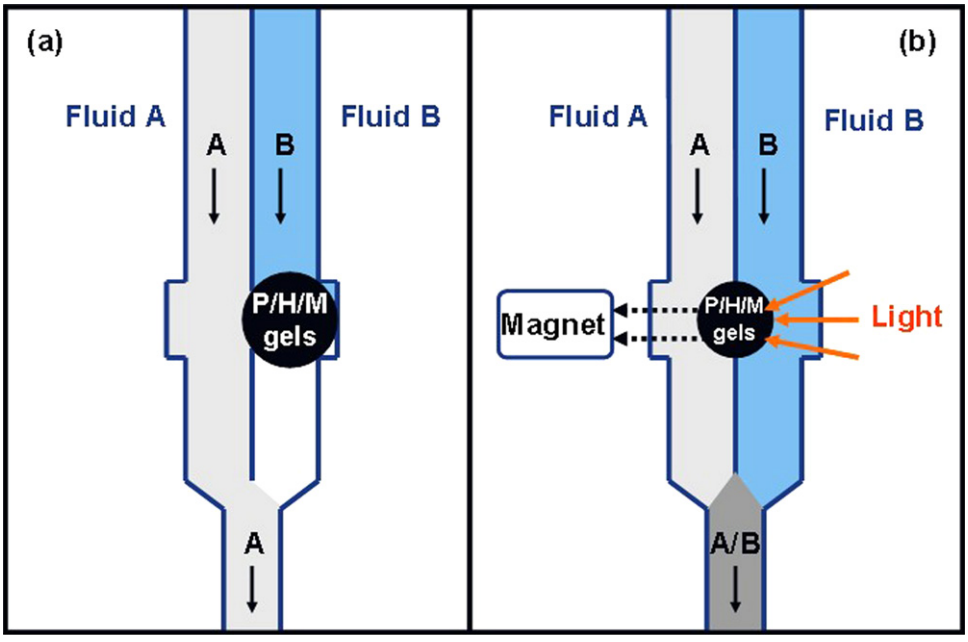

Fig. 9. Schematic diagram of the application of P/H/M gels switch in microreactors. (a) Fluid B channel is off; (b) both fluid A and fluid B channels are on, the ratio of the two kind of fluid is tuned to 1:1.

surface energy. Furthermore, PEG 200 could prevent fast growth of crystallites and could be helpful toward achieving oriented aggregation [24].

3.4. Magnetic studies

The magnetic hysteresis curves of MWCNTs/$Co_{1-x}Zn_xFe_2O_4$ magnetic nanocomposites were recorded by sweeping the external field between ±4 kOe at room temperature. Fig. 5 shows the room temperature magnetic hysteresis loops of the powder samples for various zinc substitutions. The saturation magnetization value of the MWCNTs/$Co_{1-x}Zn_xFe_2O_4$ magnetic nanocomposites (x = 0.2, 0.4, 0.5, 0.6, 0.8) were 56.6, 57.4, 57.5, 53.2 and 48.1 emu g^{-1}, respectively. The inserted photo shows the MWCNTs/$Co_{1-x}Zn_xFe_2O_4$ magnetic nanocomposites placed in an external magnetic field. The magnetic nanocomposites were attracted to the magnet (located on the left side of sample vials) in a relatively short period, demonstrating the high magnetic sensitivity of our products.

In the cubic system of ferromagnetic spinels, the magnetic order is mainly due to a super exchange interaction mechanism occurring between the metal ions in the A and B sublattices. The substitution of nonmagnetic ions such as Zn, which has a preferential A site occupancy results in the reduction of the exchange interaction between A and B sites. Hence, by varying the degree of zinc substitution, it is possible to manipulate the magnetic properties of the fluid samples [17,20]. According to Neel's two sublattice model of ferrimagnetism, the magnetic moment per formula unit in μ_B, $n^BN(x)$ is expressed as:

$$n^BN(x) = M_B(x) - M_A(x)$$

where M_B and M_A are the B- and A-sublattice magnetic moment in μ_B respectively [34].

The changes in the saturation magnetization with the degree of Zn^{2+} substitution are given in Fig. 6. It is observed that the saturation magnetization of the MWCNTs/$Co_{1-x}Zn_xFe_2O_4$ magnetic nanocomposites increases when the Zn^{2+} content is lower than 0.5, but decreases rapidly when the Zn^{2+} content is higher than 0.5. The saturation magnetization as a function of Zn^{2+} substitution reaches a maximum value of 57.5 emu g^{-1} for x = 0.5. This could be due to Zn^{2+} (with zero magnetic moment) replaced the ions on the octahedral A-sites, causing the decrease of magnetic moment in the sublattice M_A, resulting in the increase of total magnetic moment for $x \leq 0.5$. However, the saturation magnetization of the MWCNTs/$Co_{1-x}Zn_xFe_2O_4$ magnetic nanocomposites decreases rapidly when the Zn^{2+} content is larger than 0.5. This could be due to further increase in the concentration of Zn^{2+} (more than 0.5). The exchange interaction between A and B sites gets lowered, which strengthening the interaction of B–B and weakening the interaction of A–B simultaneously. It could leads to the decrease of saturation magnetization [34]. Fig. 2 shows that X-ray density increases with increasing Zn^{2+} content, which confirms that the Zn^{2+} replaced the ions on the octahedral A-sites.

The temperature dependence of zero field cooled (ZFC) and field cooled (FC) magnetization of MWCNTs/$Co_{0.5}Zn_{0.5}Fe_2O_4$ nanocomposite is shown in Fig. 7. The data of the sample were recorded in the presence of 100 Oe applied field at the temperature range of 2–300 K. The result (Fig. 7) shows that the ZFC magnetization decreases continuously, which indicates that the blocking temperature of the sample is above the room temperature such that the sample shows ferromagnetic behavior at all measurement temperatures [18].

3.5. Application of P/H/M gels

PNIPAAm/MWCNTs/$Co_{1-x}Zn_xFe_2O_4$ hydrogels were prepared by simple mixing and solution polymerization. The as-prepared hydrogels are shown in Fig. 8a. In Fig. 8b and c, it can be clearly seen that the P/H/M gels exhibit a good response to the external magnet, which are expected to be used as a light-driven and magnetic controlled switch in microreactors. A schematic of the application of P/H/M gels switch in microreactors is shown in Fig. 9. Upon irradiation with light, the P/H/M gels deswelled and contracted, the ratio of the two kinds of fluid could be finely controlled by changing the position of the P/H/M gels switch with a magnet (as shown in Fig. 9a and b).

4. Conclusions

A suitable preparation technique for MWCNTs/$Co_{1-x}Zn_xFe_2O_4$ magnetic nanocomposites is reported. MWCNTs/$Co_{1-x}Zn_xFe_2O_4$ magnetic nanocomposites can be prepared by the solvothermal method for the range of composition with x varying from 0.2 to 0.8. TEM images show that a large number of $Co_{1-x}Zn_xFe_2O_4$ nanocrystals are aggregated around the sidewalls of MWCNTs. Magnetic studies indicate that the saturation magnetization of these nanocomposites increases when the Zn^{2+} content is lower than 0.5, but decreases rapidly when the Zn^{2+} content is higher than 0.5. The saturation magnetization as a function of Zn^{2+} substitution reaches a maximum value of 57.5 emu g^{-1} for x = 0.5. Furthermore, these nanocomposites display a high magnetic sensitivity and have a high saturation magnetization. PNIPAAm/MWCNTs/$Co_{1-x}Zn_xFe_2O_4$ hydrogels were prepared by simple mixing and solution polymerization. The as-prepared hydrogels are expected to be used as a light-driven and magnetic controlled switch in microreactors.

Acknowledgements

We gratefully acknowledge the financial supports by Ministry of Education of the People's Republic of China (No. NECT-05-0419), Shanghai Municipal Education Commission (No. 07SG37), Natural Science Foundation of China (Nos. 50772022, 50772127), Shanghai Leading Academic Discipline Project (B603), the Cultivation Fund of the Key Scientific and Technical Innovation Project (No.708039), and the Program of Introducing Talents of Discipline to Universities (No. 111-2-04).

Appendix A. Supplementary data

Supplementary data associated with this article can be found, in the online version, at doi:10.1016/j.jallcom.2011.01.018.

References

[1] I. Capek, Adv. Colloid. Interface 150 (2009) 63–89.
[2] E. Lidorikis, A.C. Ferrari, ACS Nano 3 (2009) 1238–1248.
[3] D. Tasis, N. Tagmatarchis, A. Bianco, M. Prato, Chem. Rev. 106 (2006) 1105–1136.
[4] V.N. Popov, Mater. Sci. Eng. R 43 (2004) 61–102.
[5] D. Eder, Chem. Rev. 110 (2010) 1348–1385.
[6] C.Q. Feng, L. Li, Z.Q. Guo, H. Li, J. Alloys Compd. 504 (2010) 457–461.
[7] F. Teng, S. Santhanagopalana, Y. Wang, D.D. Meng, J. Alloys Compd. 499 (2010) 259–264.
[8] Y.P. Zhang, X.W. Sun, L.K. Pan, H.B. Li, Z. Sun, C.Q. Sun, B.K. Tay, J. Alloys Compd. 480 (2009) L17–L19.
[9] H. Xu, Y.B. Pan, Y. Zhu, H.M. Kou, J.K. Guo, J. Alloys Compd. 481 (2009) L4–L7.
[10] C.N. He, F. Tian, S.J. Liu, J. Alloys Compd. 478 (2009) 816–819.
[11] K.J. Lee, Y.T. Yeh, H.Z. Cheng, P.C. Chang, S.W. Lin, Y.D. Chen, J. Alloys Compd. 504S (2010) S356–S360.
[12] T.G. Mathe, T. Moyo, J.Z. Msomi, Phys. Status Solidi C 5 (2008) 591–593.
[13] A.K.M. Akther Hossain, H. Tabata, T. Kawai, J. Magn. Magn. Mater. 320 (2008) 1157–1162.

[14] M.U. Islam, F. Aen, S.B. Niazi, M. Azhar Khan, M. Ishaque, T. Abbas, M.U. Rana, Mater. Chem. Phys. 109 (2008) 482–487.
[15] G. Vaidyanathan, S. Sendhilnathan, Physica B 403 (2008) 2157–2167.
[16] G.V. Duong, N. Hanh, D.V. Linh, R. Groessinger, P. Weinberger, E. Schafler, M. Zehetbauer, J. Magn. Magn. Mater. 311 (2007) 46–50.
[17] G. Vaidyanathan, S. Sendhilnathan, J. Magn. Magn. Mater. 320 (2008) 803–805.
[18] F. Gözüak, Y. Köseoğlu, A. Baykal, H. Kavas, J. Magn. Magn. Mater. 321 (2009) 2170–2177.
[19] J.S. Ghodake, R.C. Kambale, S.V. Salvi, S.R. Sawant, S.S. Suryavanshi, J. Alloys Compd. 486 (2009) 830–834.
[20] G. Vaidyanathan, S. Sendhilnathan, R. Arulmurugan, J. Magn. Magn. Mater. 313 (2007) 293–299.
[21] N.M. Burange, S.S. Chougule, D.R. Patil, R.S. Devan, Y.D. Kolekar, B.K. Chougule, J. Alloys Compd. 479 (2009) 569–573.
[22] V.G. Patil, S.E. Shirsath, S.D. More, S.J. Shukla, K.M. Jadhav, J. Alloys Compd. 488 (2009) 199–203.
[23] A.S. Fawzi, A.D. Sheikh, V.L. Mathe, J. Alloys Compd. 493 (2010) 601–608.
[24] C. Hou, H. Yu, Q. Zhang, Y. Li, H. Wang, J. Alloys Compd. 491 (2010) 431–435.
[25] D. Shi, J.P. Cheng, F. Liu, X.B. Zhang, J. Alloys Compd. 502 (2010) 365–370.
[26] C.-H. Chen, Y.-H. Liang, W.-D. Zhang, J. Alloys Compd. 501 (2010) 168–172.
[27] W. Jiang, Y. Liu, F. Li, J. Chu, K. Chen, Mater. Sci. Eng. B 166 (2010) 132–134.
[28] F.R. Lamastra, F. Nanni, L. Camilli, R. Matassa, M. Carbone, G. Gusmano, Chem. Eng. J. 162 (2010) 430–435.
[29] Y. Liu, W. Jiang, L. Xu, X. Yang, F. Li, Mater. Lett. 63 (2009) 2526–2528.
[30] Q. Zhang, M.F. Zhu, Q.H. Zhang, Y.G. Li, H.Z. Wang, Mater. Chem. Phys. 116 (2009) 658–662.
[31] K. Haraguchi, T. Takehisa, S. Fan, Macromolecules 35 (2002) 10162–10171.
[32] Y. Liu, M. Zhu, X. Liu, W. Zhang, B. Sun, Y. Chen, H.-J.P. Adler, Polymer 47 (2006) 1–5.
[33] B. Jia, L. Gao, J. Sun, Carbon 45 (2007) 1476–1481.
[34] S. Singhal, T. Namgyal, S. Bansal, K. Chandra, J. Electromagn. Anal. Appl. 2 (2010) 376–381.